

PERFORMANCE ANALYSIS OF WDM-PON ARCHITECTURE FOR WIRELESS SERVICES DISTRIBUTION IN FUTURE AIRCRAFT NETWORKS

D. Coelho^{1,2}, J.M.B Oliveira¹, L.M.Pessoa^{1,2}, H.M. Salgado¹ and J.C.S. Castro¹

¹*INESC TEC(formerly INESC Porto), Porto, Portugal*

²*Faculdade de Engenharia, Universidade do Porto, Porto, Portugal*
(dcoelho,joao.b.oliveira,lpessoa,hsalgado,jcastro)@inescporto.pt

Keywords: WDM, Wi-Fi, signal-to-noise ratio, error vector magnitude and intermodulation distortion.

Abstract: In this work, an in-depth analysis concerning the transmission performance of IEEE802.11g/n (Wi-Fi) signals in a WDM-PON system is presented. It is considered that the optical/electrical transceivers are based on low-cost 850 nm VCSELs and PIN photodiodes. System modelling includes the impact of noise generated in the optical path, such as relative intensity noise (RIN), shot noise, photodetector thermal noise, clipping and intermodulation distortion. An analytic analysis based on Volterra series is conducted and mathematical expressions for both the EVM and SNR are derived. The theoretical analysis is also compared with experimental results. Among several conclusions, it is observed that the laser intermodulation distortion, clipping and RIN are the most relevant factors.

1 INTRODUCTION

In the last decade, wireless communications have experienced a great expansion and the demand for higher data traffic to accommodate the new services, like VoIP (Voice over IP), IPTV (Internet Protocol Television) or Video on Demand (VoD) and peer-to-peer (P2P) have increased quickly. One application domain in which wireless networks can obtain additional use is in aviation, since there is the need for connectivity and network services “every time” and “everywhere”. Another important factor is that commercial aircraft operators are currently looking for ways to attract more customers by increasing the value of their service offerings to passengers [1].

In the future, in-flight entertainment (IFE) services should offer to passengers high speed wireless internet connectivity, using their own personal computers as if they were earthbound [1]. Entertainment services can comprise digital video and audio services, such as high definition (HD) video on demand, music, and satellite HDTV.

Figure 1, depicts a scheme of a possible future optical fiber based network suitable for aircraft cabins, where the communication signals between the aircraft, ground and satellite stations are represented.

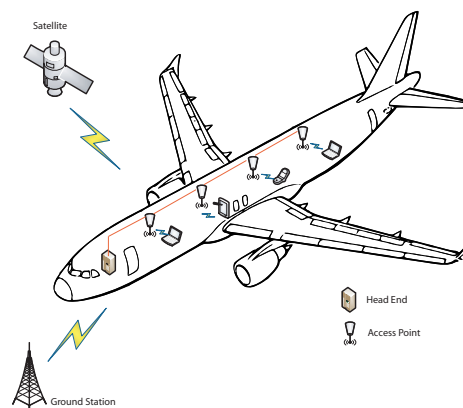


Figure 1: Scheme of the aircraft communication system.

PONs are quickly becoming one of the most popular access systems in telecommunications. Wireless and fixed access convergence over PONs, are also topics of much debate [2]. They can be used to provide wireless communication services in these networks due to its high bandwidth and without electromagnetic interference. Moreover, using WDM there is a simplification, compared to TDM PONs, of the network topology by allocating different wavelengths to individual optical network terminator (ONT).

PONs can transparently deliver multiple services such as IEEE 802.11(Wi-Fi), global system for mobile communications (GSM), WiMAX or ultra-wide band (UWB).

IEEE 802.11 or Wireless-Fidelity (Wi-Fi) is a set of standards for implementing Wireless Local Area Network (WLAN) data communication in the 2.4 and 5 GHz frequency range. IEEE 802.11g works in the 2.4 GHz frequency band and uses OFDM signals with 20MHz of bandwidth and power signal of 0dBm/MHz. The subcarriers can be QPSK, 16-QAM or 64-QAM. The IEEE 802.11n standard adds the use of the Multiple-Input Multiple-Output (MIMO) technology and operates in the 2.4 GHz and 5.0 GHz bands with 40-MHz bandwidth. Orthogonal Frequency Division Multiplexing (OFDM) is a multicarrier modulation scheme that is well known due to its robustness in multipath fading channels. Yet, due to its high peak-to-average power ratio, OFDM is susceptible to nonlinear distortion from components such as optical modulators and directly modulated diode lasers [5].

A low cost solution for these systems involves the use of directly modulated Vertical Cavity Surface Emitted Lasers (VCSELs). These lasers are characterized by a vertical low divergence, circular beam patterns, low threshold currents (a few mA) and high bandwidths (several GHz). Their vertical wafer growth process enables in-wafer testing, and is well suited for large scale production. These are reasons that make VCSELs desirable for low cost directly modulated systems in these types of widespread commercial applications [3].

This article is divided in seven sections. Section 2 describes briefly the WDM-PON topology. Section 3 addresses the interference generated by source nonlinearities. Section 4 presents the laser model. Section 5 presents discusses the system performance analysis including all noise contributions and laser distortions at the receiver. The results are presented in Section 6 with the comparison between simulation and experimental results. Finally, Section 7 highlights the main conclusions.

2 WDM-PON

Wavelength-division-multiplexed passive optical networks (WDM-PON) offer many advantages such as large capacity, easy management, network security, and upgradability. The usage of an array waveguide grating (AWG) to multiplex/de-multiplex the upstream and downstream wavelengths, respectively, provides a dedicated point-to-point optical channel

between each ONT and the optical line terminator (OLT), although this concept involves the sharing of a common point-to-multipoint physical architecture [4]. Since a wavelength mux/demux is used instead of an optical-power splitter, the insertion loss is considerably smaller and effectively independent of the splitting ratio. In addition, since the receiver bandwidth for each ONT is matched to its dedicated bandwidth, there is no additional penalty related to the number of users on the PON [4]. Consequently, the signal-to-noise ratio (SNR) is essentially independent of the number of ONTs, allowing efficient scaling and flexibility for a WDM-PON architecture, which is suited to transport multiple wireless standards including Wi-Fi.

A WDM-PON scheme representation is depicted in Figure 2. In this architecture, each ONT-OLT pair is assigned a set of downstream and upstream wavelengths.

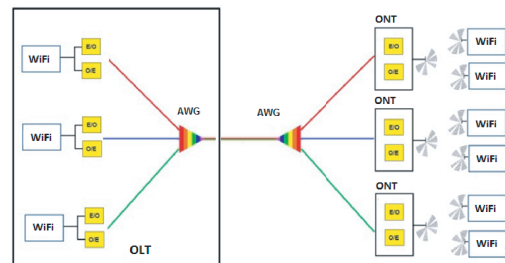


Figure 2: WDM-PON Scheme.

An additional feature of a WDM architecture is its ability to localize any fault or optical loss in the fiber plant by using a single wavelength-tunable OTDR (optical time-domain reflectometer) located at the OLT.

AWGs require temperature control to keep their optical channels locked to a wavelength grid. Technology advances have allowed the recent commercialization of athermal AWGs that can remain locked to a WDM-wavelength grid over temperature ranges experienced at the passive-node location [4].

3 INTERMODULATION DISTORTION

Due to the large number of electrical subcarriers of the WiFi signal, a high nonlinear distortion may be expected from the electrical to optical conversion when using direct modulated laser diodes, such as VCSELs.

The interference resulting from source nonlinearity depends strongly on the number of channels and the distribution of channel frequencies. Considering

the transmission of three channels (f_1 , f_2 and f_3), Figure 3 shows the harmonics generated by a nonlinear device.

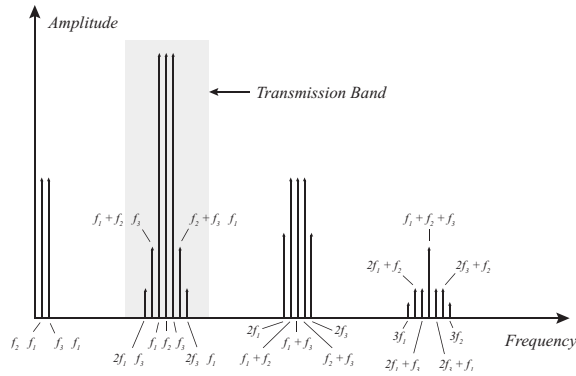


Figure 3: Illustration of harmonics generated by a nonlinear optical modulator [5].

The most troublesome third-order intermodulation distortion products (IMPs) are those that originate from frequencies $f_i + f_j - f_k$ and $2f_i - f_j$, and since they lie in within the transmission band, they lead to interchannel interference. The interference, thus, depends strongly on the number of channels and on the allocation of channel frequencies with respect to the resonance frequency of the laser. For a n channels system with uniform frequency spacing the number of IMPs, rIM_{21}^n and rIM_{111}^n of type $2f_i - f_j$ and $f_i + f_j - f_k$, respectively, coincident with channel r are given by [6].

$$rIM_{21}^n = \frac{1}{2} \left\{ n - 2 - \frac{1}{2} [1 - (-1)^n] (-1)^r \right\} \quad (1)$$

$$rIM_{111}^n = \frac{r}{2} (n - r + 1) + \frac{1}{4} [(n - 3)^2 - 5] - \frac{1}{8} [1 - (-1)^n] (-1)^{n+r} \quad (2)$$

Considering a WiFi system, the total number of channels is equals $n = 64$. Figure 4 shows the total number of third-order IMPs as a function of channel number. The channel in the middle of the band is the one with the large number of intermodulation products.

4 LASER MODEL

4.1 Intrinsic Model

The laser operation is described by the relationship between the carrier density N and the photon density

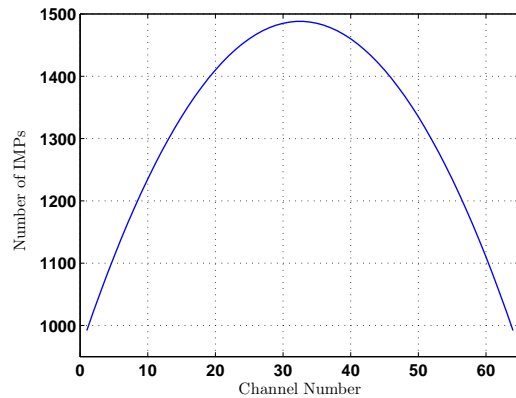


Figure 4: Total number of third-order intermodulation products for $n=64$.

S under the presence of the injected current I . This is accomplished through a set of rate equations that explain all the mechanisms by which the carriers are generate or lost inside the active region. this set of equations is defined by [7]:

$$\frac{dN}{dt} = \frac{\eta_i I}{qV} - \frac{N}{\tau_n} - g_0 (N - N_{0m}) (1 - \epsilon S) \quad (3)$$

$$\frac{dS}{dt} = \Gamma g_0 (N - N_{0m}) (1 - \epsilon S) S - \frac{1}{\tau_p} S + \beta \Gamma \frac{N}{\tau_n} \quad (4)$$

The first term in (3) is the rate at which the carriers, electrons or holes are injected into the active layer due to current I . The second term in the equation is the loss due to various recombination process (spontaneous and nonraditive emission) and the last term is due to the stimulated emission recombination that leads to the emission of light. The equation (4) states that the rate of increase in photon density is equal to the photon generation by stimulated emission less the loss rate of photons (as characterized by the photon lifetime, τ_p), plus the rate of spontaneous emission.

The parameter V is the active region volume, g_0 is the gain slope constant, ϵ is the normalized gain compression factor, N_{0m} is the electron density at transparency, β is the fraction of the total spontaneous emission coupled at the laser mode, Γ is the optical confinement factor, η_i is the injection efficiency, τ_p is the photon lifetime and τ_n is the carrier lifetime.

The optical output power can be expressed as $P = \eta h \nu S$, where $\eta = (\eta_d V) / (2 \Gamma \eta_i \tau_p)$, h is the Planck's constant, ν is the emission frequency and η_d is the differential quantum efficiency.

In this work, the VCSEL model FINISAIR HFE-4192-582, operating at 850 nm, was used. The intrinsic parameters extracted, by the frequency subtraction method [8], were then used in the simulation model (see Table 1).

Parameter	Value	Unit
V	2.4×10^{-18}	m^3
g_0	4.2×10^{-12}	$m^3 s^{-1}$
ϵ	2.0×10^{-23}	m^3
N_{0m}	1.9×10^{24}	m^{-3}
β	1.7×10^{-4}	—
Γ	4.5×10^{-2}	—
τ_p	1.8	ns
τ_n	2.6	ps
η_i	0.8	—

Table 1: Intrinsic parameters of FINISAIR HFE-4192-582.

Since the laser dynamics described by the rate equations are intrinsically nonlinear, harmonic and intermodulation distortion occurs during direct modulation which limits system performance. Modelling of the semiconductor laser diode in such a way as to render tractable the accurate computation of intermodulation products (IMPs) is thus of importance for the design and dimensioning of such systems.

4.2 Package and Chip Parasitics Model

In the laser model we will consider an intrinsic laser diode (ILD), whose dynamic behavior is described by the previous rate equations (equation 3 and 4) and a parasitic interconnection circuit due to the laser assembly in a package. The corresponding equivalent electrical circuit of the parasitics elements of the FINISAIR HFE-4192-582 is shown in Figure 5.

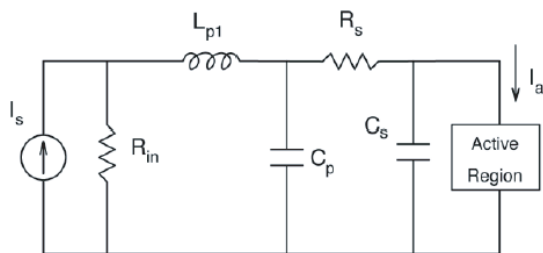


Figure 5: Parasitic model.

Table 2 presents the intrinsic laser parameters of the VCSEL operating at 850 nm. Combining the parameters obtained for the parasitic circuit and the intrinsic laser model, the global transfer function is obtained as can be seen in Figure 6.

The relative noise intensity characteristic of this VCSEL, was obtained from the rate equation with Langevin noise sources been represented in Figure 7. In the range of 3 to 9 mA RIN varies between -152 to -133 dB/Hz.

Parameter	Value	Unit
R_{in}	50	Ω
R_s	42.6279	Ω
C_s	0	ps
C_p	1.8068	pF
L_{p1}	7.6925	pF

Table 2: Parasitic parameters of FINISAIR HFE-4192-582.

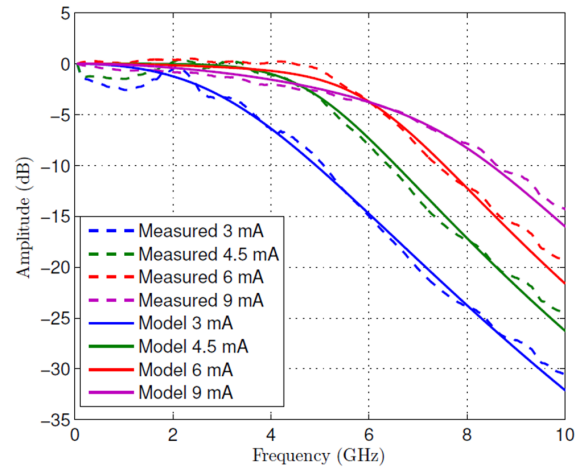


Figure 6: Frequency response of FINISAIR HFE-4192-582.

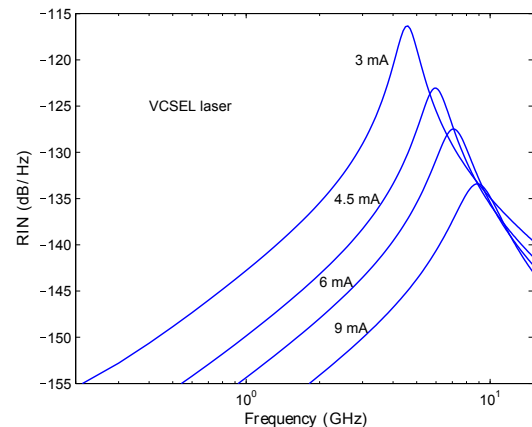


Figure 7: Relative Intensity Noise of the VCSEL.

5 ARCHITECTURE ANALYSIS

The maximum fiber length of an optical network to be deployed inside an aircraft is considered to be 100 meters. Thus, it is reasonable to neglect both the attenuation and dispersion of RF signals with frequencies up to 10 GHz [9].

As aforementioned, WDM architecture provides a dedicated point-to-point optical channel between each ONTs and the OLT. Taking this into account let us consider the point-to-point architecture shown in the Figure 8. Since the RF signal which arrives at the antenna is a weak signal due to the wireless attenuation,

the SNR in the uplink is considerably lower than in the downlink.

The RF uplink signal is generated by the Mobile Station and reaches the base station attenuated by the wireless channel. The weak RF uplink signal is then electrically amplified (G) before being converted from the electrical to the optical domain by the VCSEL. In the central station, the optical signal is detected by a PIN photodetector which converts the optical signal to the electrical before reaching the Wi-Fi receiver module (WiFi Rx). The RF signal detected will suffer the impact of the RIN noise, shot noise, photodetector thermal noise, clipping and intermodulation distortion.

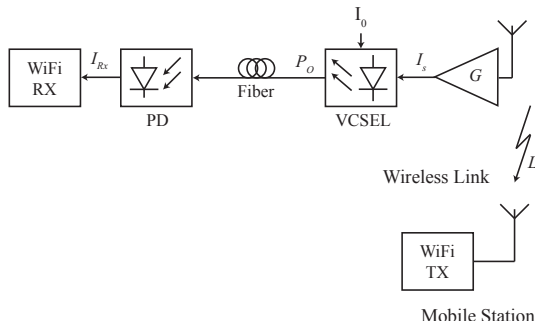


Figure 8: Point-to-point transmission scheme.

The SNR for the uplink path, referred at the output of the photodiode optical receiver, can be written as [10],

$$SNR = \frac{\langle I_{Rx}^2 \rangle}{\langle I_{RIN}^2 \rangle + \langle I_{SN}^2 \rangle + \langle I_{th}^2 \rangle + \langle I_{IMD}^2 \rangle + \langle I_{clp}^2 \rangle} \quad (5)$$

where the five current noise terms are: the RIN noise current, the shot noise current, the thermal noise current from the equivalent resistance of the photodetector (PD) load and amplifier (R_{eq}), the current due to the third order intermodulation distortions and the current due clipping distortions, respectively. The source thermal noise can be neglected and $\langle I_{Rx}^2 \rangle$ is the signal power at the receiver as described in [9][10][11].

$$\langle I_{Rx}^2 \rangle = \frac{1}{2} \left(r_d \mu \sqrt{\frac{2}{N}} \langle P_0 \rangle \right)^2 \quad (6)$$

$$\langle I_{RIN}^2 \rangle = r_d^2 \langle P_0^2 \rangle 10^{\frac{RIN}{10}} \Delta f \quad (7)$$

$$\langle I_{SN}^2 \rangle = 2q r_d \langle P_0 \rangle \Delta f \quad (8)$$

$$\langle I_{th}^2 \rangle = \frac{4kTF\Delta f}{R_{eq}} \quad (9)$$

$$\langle I_{IMD}^2 \rangle = \frac{(r_d \langle P_0 \rangle)^2}{2} \left(\mu \sqrt{\frac{2}{N}} \right)^6 (D_{111} N^2 + D_{21} N) \quad (10)$$

$$\langle I_{clp}^2 \rangle = \frac{1}{\sqrt{2\pi}} \Lambda r_d \langle P_0 \rangle \frac{\mu^5}{1 + 6\mu^2} e^{-\frac{1}{2}\mu^2} \quad (11)$$

The r_d parameter is the photodetector responsivity, P_0 is the average optical power detected by the PD, Δf is the electrical bandwidth of the receiver, q is the electronic charge (1.6×10^{-19} Coulomb), k is the Boltzmann's constant, $T = 290K$, F is the noise factor of the amplifier following the PD and D_{111} and D_{21} are the third-order distortion coefficients (IMDs $f_i + f_j - f_k$ and $2f_i - f_j$), which depend on the laser characteristics and operation point. The μ parameter is the total rms modulation index and is equal to $\mu = m \sqrt{N/2}$, where m is the optical modulation index per subcarrier [11]. The Λ parameter represents the fraction of the clipping distortion power which falls in the transmission band which is also dependent on the optical modulation index [12]. For the specific channel allocation, $\Lambda = 1.1 \times 10^{-3}$ for $\mu = 2\%$.

6 SIMULATIONS AND RESULTS

The presented analysis considers the usage of Wi-Fi signals in the 2.4 GHz frequency range, with 20 MHz of bandwidth and the use of OFDM with 64 orthogonal subcarriers ($N = 64$). Here we have assumed that the signal directly modulates a VCSEL.

Volterra functional series, described as a “power series with memory”, has been applied previously to assess accurately the laser distortion of the semiconductor laser [13]. The latter analysis enables one to determine adequately the third-order intermodulation coefficients of the semiconductor laser, considering the allocation of subcarriers for Wi-Fi.

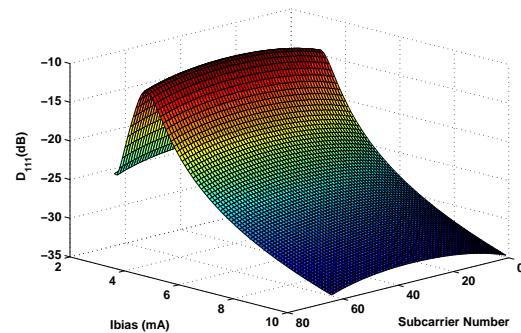


Figure 9: D_{111} for several bias current.

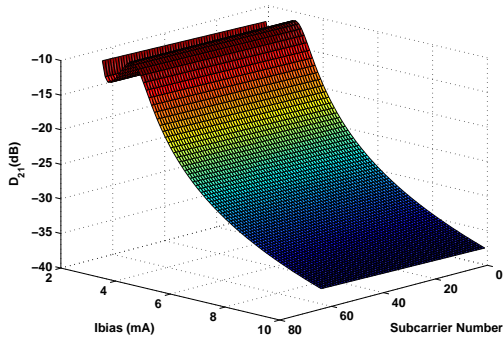


Figure 10: D_{21} for several bias current.

The D_{111} coefficient has the major impact in the IMD limitation since it increases with N^2 , while the D_{21} contribution increases with N (eq. 10). Also from Figures 9 and 10, it is seen that a better performance is expected when the VCSEL is operated at 9 mA of bias current and a worst performance at 3 mA, when considering the IMD impact on the system performance. For a bias current of 3 and 5 mA, D_{111} is maximum for the subcarrier number 34 and 35, and equals 0.0522 and 0.0057, respectively. The corresponding maximum values for D_{21} occur for subcarrier number 63 and 64, and are 0.0081 and 0.0034, respectively. The resonance of the laser may actually change the location within the band (subcarrier) where we would expect the maximum distortion to occur (middle channel for D_{111} and last channel for D_{21}).

The previous theoretical analysis, based on SNR, is compared with experimental results. Experimentally the performance of the system is assessed in terms of error vector magnitude (EVM), which relates to the SNR by [14].

$$EVM_{rms} = \frac{1}{\sqrt{SNR}} \quad (12)$$

The experimental setup used is depicted in Figure 11. It is composed of a vector signal generator (RODHE&SCHWARZ SMJ 100A) to generate the Wi-Fi signal, an electrical to optical converter (VCSEL model FINISAIR HFE-4192-582), an optical to electrical converter (81495A) and a Digital Serial Analyzer (Tektronics DSA 71254C) for the signal analysis and EVM measurements. The VCSEL laser has a slope efficiency of 0.075 W/A and a threshold current of 0.8 mA and the PIN photodetector is considered to have a responsivity of 50 A/W.

Figures 12 and 13 show the results of both analytical and experimental SNR as a function of the total rms modulation index, for the uplink point-to-point

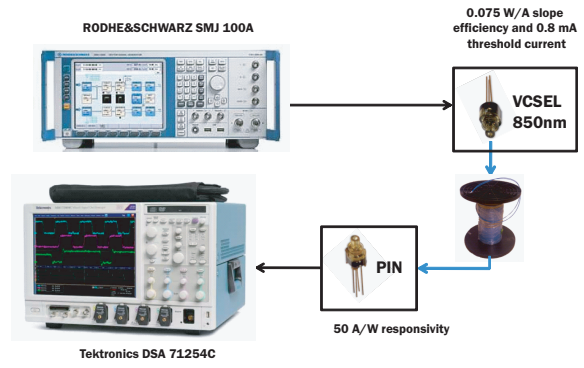


Figure 11: Diagram of experimental setup.

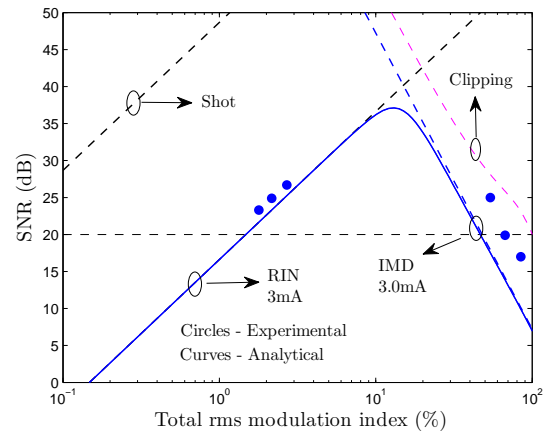


Figure 12: Analytical and experimental SNR $I_{Bias} = 3$ mA.

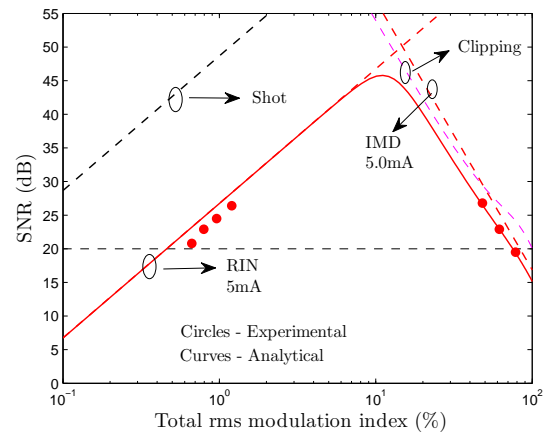


Figure 13: Analytical and experimental SNR $I_{Bias} = 5$ mA.

transmission scheme. The noise limiting contributions are plotted in the graph as well. A minimum SNR of 20 dB can be specified considering a typical sensitivity from a commercial IEEE 802.11n of -74 dBm, in the 2.4 GHz band [15]. From the results we can see that the best performance in terms of SNR is achieved at high bias currents, when the intermodulation distortion is lower and the performance is lim-

ited by both clipping and IMD. The maximum SNR value for a bias current of 3 mA is 37.12 dB for a total rms modulation index of 13%, while for a bias current of 5 mA, the maximum SNR is 45.78 dB for a total rms modulation index of 11%. Measurements of SNR above 30 dB were not obtained, since the results show a tendency to reach a plateau, which indicate that as the RF input power increases, the photoreceiver's amplifier limits the power of the signal, which on the other hand limits the SNR.

Let us consider now an analysis for a network with higher fiber length, which can be applied for other WDM-PON network architectures. Note that these new results are obtained taking only into consideration the optical loss due to fiber attenuation. From equation 5 and for $I_{Bias} = 5$ mA the SNR versus the total rms optical modulation index for several values of attenuation ($\alpha = 3, 6, 9, \dots, 24$ dB) is plotted in Figure 14. We can see that for low modulation indexes values the SNR performance is limited mainly by thermal noise except for the $\alpha = 0$ dB case, where the RIN is the leading noise source.

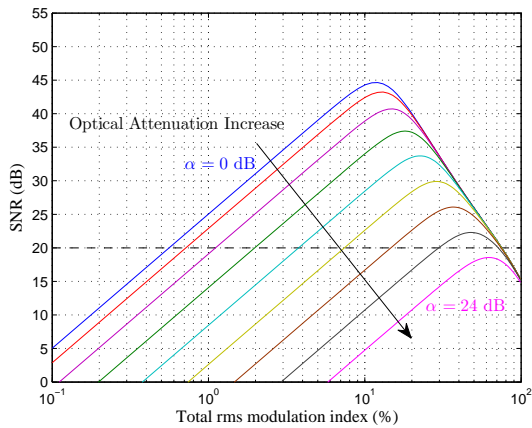


Figure 14: SNR as a function of the total rms modulation index for different optical attenuation values ($I_{Bias} = 5$ mA).

In Figure 15 it is depicted the maximum SNR values and the corresponding modulation indexes as a function of the optical attenuation. These modulation indexes are considered to be optimum in the SNR sense. The results indicates that the maximum optical attenuation that can be considered for an acceptable minimum SNR of 20 dB is $\alpha = 23$ dB (for $I_{Bias} = 5$ mA). By considering a multimode fiber with an attenuation of 3 dB/Km at 850 nm, it corresponds to 7.7 Km.

By considering a minimum SNR of 20 dB for a reliable transmission, it is possible to determine from Figure 14 the corresponding minimum modulation index (and minimum electrical power) of the RF signal that drives the VCSEL. This result gives us the mini-

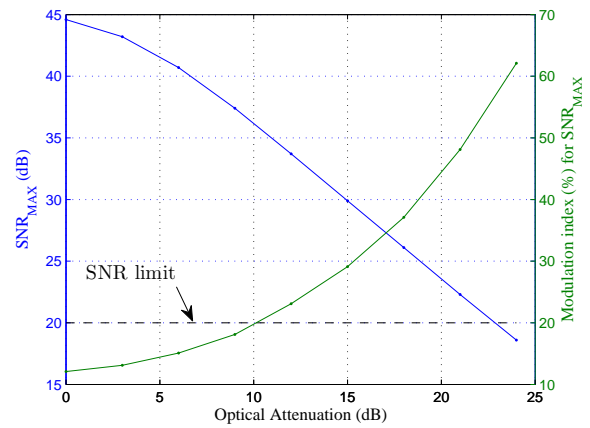


Figure 15: Maximum SNR and optimum modulation index values as a function of the optical attenuation ($I_{Bias} = 5$ mA).

imum RF power that can be used to directly modulate the VCSEL for an SNR of 20 dB. Figure 16 shows this result as a function of the optical attenuation.

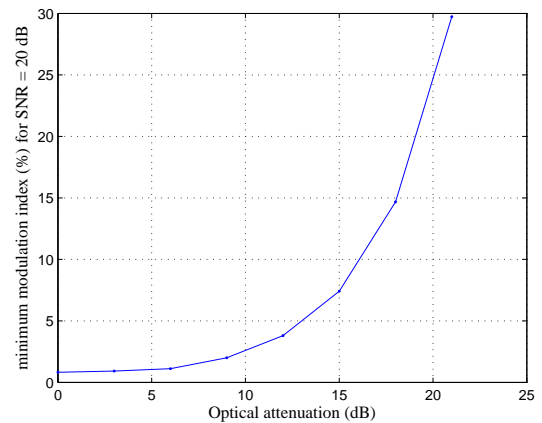


Figure 16: Minimum modulation index value to achieve an acceptable SNR of 20 dB as a function of the optical attenuation ($I_{Bias} = 5$ mA).

Assuming an RF signal with power given by

$$P_{RF} = \frac{1}{2} \langle I^2 \rangle R_i \quad (13)$$

where R_i is the input resistance of the VCSEL considered to be 50Ω , the relation between RF power and modulation index is plotted in Figure 17.

Considering a maximum amplifier gain (G) of 30 dB and assume that the antenna noise from the ONT does not severely affect the SNR of the signal, the RF power at the input of the VCSEL is given by:

$$P_{in} = P_{TX,max} - L + G + 4 \quad (14)$$

where $P_{TX,max} = 13$ dBm is the maximum transmitter power defined by the standard, L is the wireless FSPL

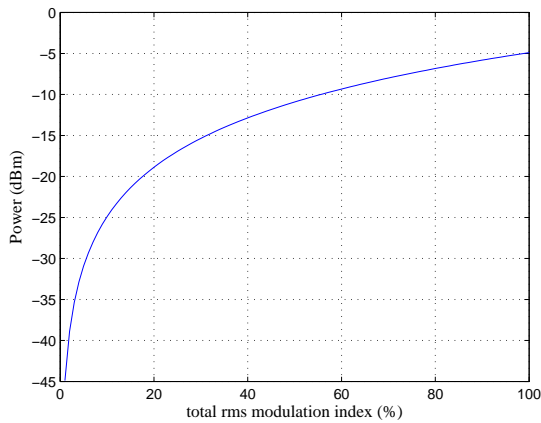


Figure 17: RF power as a function of the modulation index ($I_{Bias} = 5$ mA).

(Free Space Path Loss) defined by:

$$FSPL(dB) = 20\log_{10}(d) + 20\log_{10}(f) - 147.55 \quad (15)$$

where d is the wireless link length in meters and f is the RF signal frequency in Hertz.

Additionally, the maximum wireless link length as a function of the optical link attenuation and optical link length for an SNR = 20 dB necessary for a reliable transmission are plotted in Figures 18 and 19, respectively.

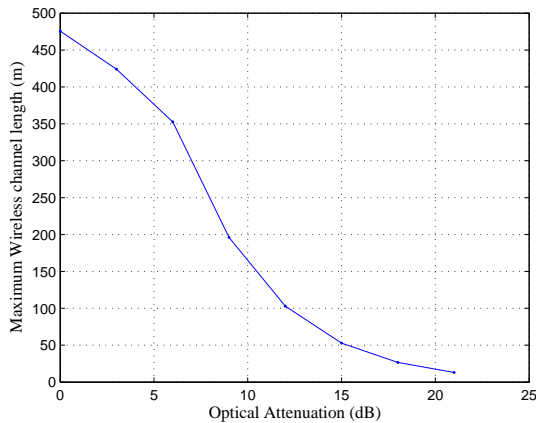


Figure 18: Maximum wireless link length as a function of the optical attenuation for a reliable transmission.

As aforementioned, the maximum fiber length of an optical network to be deployed inside an aircraft is considered to be 100 meters ($\alpha = 0$ dB case). Looking at the results, for a reliable Wi-Fi transmission, the system could be deployed with just one access point (or ONT), however if another services (WiMAX, UWB, etc) were integrated there would be necessity to increase the number of ONTs to achieve its SNR requirements.

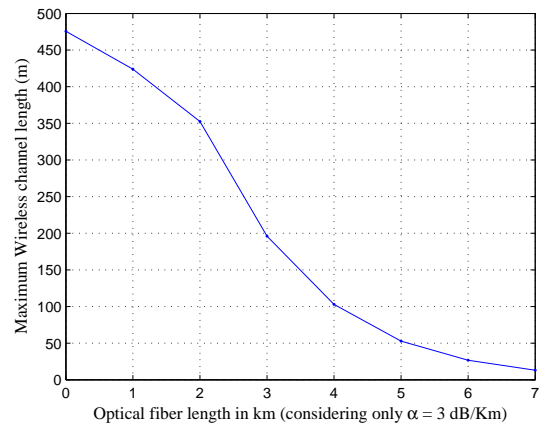


Figure 19: Maximum wireless link length as a function of the optical fiber length for a reliable transmission.

7 CONCLUSION

In this article, we have considered the transmission of WiFi signals through an optical channel. In particular, we analyze the uplink performance in a point-to-point transmission system for short range networks. A theoretical analysis was performed and a good agreement with the experimental results was obtained.

Both analytical and experimental results show that, for low bias currents, the intermodulation distortion is the main limiting performance factor at high modulation indexes, whereas the RIN is the dominant factor for low modulation indexes. For increasing bias current, the IMD distortion decreases and clipping distortion starts to dominate over intermodulation distortion, at high modulation indexes.

For a maximum fiber length of 100 meters (aircraft network case), the best performance in terms of SNR is achieved at high bias currents. The maximum SNR value for a bias current of 3 mA is 37.12 dB for a total rms modulation index of 13%, while for a bias current of 5 mA, the maximum SNR is 45.78 dB for a total rms modulation index of 11%.

For higher fiber length WDM-PON networks, the maximum optical attenuation that can be considered for an acceptable minimum SNR of 20 dB is $\alpha = 23$ dB (for $I_{Bias} = 5$ mA), which correspond a fiber length of approximately 7.7 km.

The detailed analysis and system performance presented is adequate for the assessment and design of radio-over-fiber systems in aircraft networks.

REFERENCES

- [1] INESCPorto, “Report on terrestrial networks and architectures,” tech. rep., Daphne project, 2009.
- [2] D. Qian, J. Hu, P. Ji, T. Wang, and M. Cvijetic, “10-gb/s ofdma-pon for delivery of heterogeneous services,” in *Optical Fiber Communication Conference/National Fiber Optic Engineers Conference*, p. OWH4, Optical Society of America, 2008.
- [3] J. M. B. OLiveira, S. Silva, L. Pessoa, D. Coelho, H. Salgado, and J. C. S. Castro, “Uwb radio over perfluorinated gi-pof for low-cost in-building networks,” in *Microwave Photonics (MWP), 2010 IEEE Topical Meeting on*, pp. 317–320, 2010.
- [4] C.-H. Lee, W. Sorin, and B.-Y. Kim, “Fiber to the home using a pon infrastructure,” *Lightwave Technology, Journal of*, vol. 24, no. 12, pp. 4568–4583, 2006.
- [5] J. M. B. de Oliveira, *Receiver Design for Nonlinearly Distorted OFDM Signals: Applications in Radio-over-Fiber Systems*. PhD thesis, Faculdade de Engenharia da Universidade do Porto, 2012.
- [6] R. Westcott, “Investigation of multiple f.m./f.d.m. carriers through a satellite t.w.t. operating near to saturation,” *Electrical Engineers, Proceedings of the Institution of*, vol. 114, no. 6, pp. 726–740, 1967.
- [7] H. Salgado, *Performance Assessment of Subcarrier Multiplexed Optical Systems: Implication of Laser Nonlinearities*. PhD thesis, University of Wales, 1993.
- [8] P. Morton, T. Tanbun-Ek, R. Logan, A. Sergent, P. Sciortino, and D. Coblentz, “Frequency response subtraction for simple measurement of intrinsic laser dynamic properties,” *Photonics Technology Letters, IEEE*, vol. 4, no. 2, pp. 133–136, 1992.
- [9] I. Cox, C.H., E. Ackerman, G. Betts, and J. Prince, “Limits on the performance of rf-over-fiber links and their impact on device design,” *Microwave Theory and Techniques, IEEE Transactions on*, vol. 54, no. 2, pp. 906–920, 2006.
- [10] C. H. CoxIII, *Analog Optical Links: Theory and Practice*. Cambridge University Press, 2004.
- [11] A. Saleh, “Fundamental limit on number of channels in subcarrier-multiplexed lightwave catv system,” *Electronics Letters*, vol. 25, no. 12, pp. 776–777, 1989.
- [12] J. Mazo, “Asymptotic distortion spectrum of clipped, dc-biased, gaussian noise [optical communication],” *Communications, IEEE Transactions on*, vol. 40, no. 8, pp. 1339–1344, 1992.
- [13] H. Salgado, “Modelling optical/rf impairments in ultra-wideband radio over fiber,” tech. rep., INESC Porto, 2007.
- [14] R. Shafik, S. Rahman, and R. Islam, “On the extended relationships among evm, ber and snr as performance metrics,” in *Electrical and Computer Engineering, 2006. ICECE '06. International Conference on*, pp. 408–411, 2006.
- [15] *W. N. Corporation: Product Specifications of DNMA-92, An IEEE 802.11n a/b/g/n Mini-PCI module, version 1.6, Apr. 2009.*